Stellar Population Ordering from Galactic Dynamics

Nicolas Poupart

Independent Researcher

E-mail: nicolas.poupart@yahoo.fr

Abstract. We investigate whether information on stellar population distributions can be recovered directly from galactic dynamics. Starting from observed rotation curves, we construct synthetic stellar population mixtures constrained to reproduce the effective mass distribution inferred from the dynamics. Using these reconstructed populations, we compute synthetic ultraviolet and optical colors and compare them to independent photometric observations from GALEX and SDSS.

We find statistically significant correlations between predicted and observed color indices across multiple bands, including FUV–NUV, g–r, r–z, and NUV–r. In several cases, rank–rank correlations reach significances well above 5σ, indicating that the ordering of stellar populations is robustly encoded in the dynamical information. These results suggest that galactic rotation curves carry non–trivial information about the underlying stellar population structure, beyond their traditional use as mass tracers.

Keywords: galaxies: kinematics and dynamics, galaxies: stellar populations, galaxies: photometry, ultraviolet: galaxies, methods: statistical, rotation curves

Contents

1 Introduction **1**

2 Data and Sample Selection **2**

3 Model and Predicted Quantities **3**
3.1 Stellar population reconstruction 3
3.2 Predicted photometric quantities 3
3.3 Statistical comparison and robustness tests 4

4 Results **5**
4.1 Statistical robustness of the global correlations 6
4.2 Permutation tests 7
4.3 Inclination systematics 8
4.4 Inclination-controlled subsamples 9
4.5 Morphology-controlled subsamples 9

5 Discussion **11**
5.1 Origin of the ordering 11
5.2 Limitations and scope 12

6 Conclusion **13**

A Raw predicted versus observed color relations **14**

1 Introduction

Galactic rotation curves have long played a central role in astrophysics, primarily as probes of the total mass distribution within galaxies. Their systematic deviation from expectations based on luminous matter alone has motivated the introduction of an additional mass component, commonly referred to as dark matter [1, 2]. While the physical nature of this component remains an open question, rotation curves provide a precise and well–characterized constraint on the effective gravitational mass distribution.

Stellar populations, on the other hand, are typically studied through photometric and spectroscopic observations [3]. Broadband colors, ultraviolet emission, and spectral energy distributions provide information on stellar ages, masses, and evolutionary stages. These observables are generally treated as independent from galactic dynamics, aside from indirect correlations through global galaxy properties.

In this work, we explore a different perspective: whether the information contained in galactic rotation curves is sufficient to reconstruct meaningful trends in stellar population distributions. Rather than starting from observed photometry to infer stellar content, we reverse the logic and ask whether a population mixture constrained solely by the dynamical mass distribution can reproduce observed ultraviolet and optical properties.

Our approach proceeds as follows. For each galaxy, we infer an effective mass profile from the observed rotation curve. We then construct a synthetic stellar population mixture whose

aggregate gravitational contribution reproduces this mass distribution. From the resulting population, we compute synthetic ultraviolet and optical fluxes using standard stellar parameters. Finally, we compare the predicted colors to independent observations from GALEX and SDSS.

To assess the robustness of the correspondence, we perform both Pearson and Spearman correlation analyses between predicted and observed color indices. Particular attention is given to rank–rank correlations, which test whether the relative ordering of galaxies is preserved independently of absolute calibration. The statistical significance of the correlations is quantified using Gaussian–equivalent sigma levels.

The results reveal that, across multiple color indices, the dynamical constraints within individual galaxies lead to systematically structured stellar population compositions, which translate into ordered photometric properties when compared across the galaxy sample. This finding indicates that galactic dynamics encode information about stellar population organization, even when no photometric data are used in the reconstruction. The implications of this result for the interpretation of the effective mass component and its possible energetic origin are discussed separately.

2 Data and Sample Selection

This work is based on the SPARC galaxy sample [4], which provides high-quality rotation curves derived from resolved kinematic data together with near-infrared photometry and structural parameters. All galaxies included in the SPARC database are retained in the present analysis. No selection or rejection is applied on the basis of SPARC photometric quality, since the SPARC photometry is used exclusively for the construction of rotation curves and baryonic mass distributions.

Observed galaxy colors are obtained from external ultraviolet and optical surveys. Ultraviolet photometry is taken from the GALEX mission [5, 6], while optical colors are drawn from the SDSS survey [7, 8]. As a consequence, the effective sample size is determined solely by the availability of GALEX and SDSS measurements for a given galaxy, and not by any filtering of the SPARC dataset itself. Depending on the color index considered, the number of galaxies available for the correlation analysis ranges from approximately $N \simeq 120$ to $N \simeq 140$. The exact number of objects used is explicitly reported for each color.

Four integrated color indices are analyzed in this work: $r - z$, $g - r$, FUV $-$ NUV, and NUV $- r$. Observed colors are taken directly from the GALEX and SDSS catalogues using their standard photometric calibrations. No additional extinction or inclination-dependent corrections are applied beyond those already incorporated in the original survey data.

For each galaxy, a broad set of global physical parameters is available or computable from the SPARC database, including the total baryonic mass $M_{\rm bar}$, quantities from which the dark mass component $M_{\rm dark}$ is derived, disk and bulge luminosities, mass-to-light ratios, surface brightnesses, characteristic radii, inclination angle, Hubble morphological type, and other derived photometric and kinematic quantities. In the present work, only inclination and morphological type are used as control variables for statistical robustness tests. All other global parameters are not employed in the analysis.

Predicted stellar population properties are computed independently from the observed colors, using exclusively the dynamical information encoded in the galactic rotation curves. More specifically, the reconstruction relies only on the radial distribution of the baryonic mass

and the missing mass component required to reproduce the observed dynamics, i.e. the set of points $(M_{\rm bar}(r), M_{\rm dark}(r), r)$ inferred from the rotation curve.

No photometric, spectroscopic, or stellar population information is used at any stage of the reconstruction.

From these reconstructed stellar populations, predicted integrated colors are derived. Color residuals are defined throughout this work as

$$\Delta C = C_{\rm obs} - C_{\rm pred} \tag{2.1}$$

Galaxies are grouped into three broad morphological classes based on their Hubble type, corresponding to early-type disks (S0–Sb), late-type disks (Sbc–Sdm), and irregular systems (Sm–BCD). This classification is used solely for robustness and consistency checks and does not enter the construction of the predicted stellar populations.

Galaxy inclinations i are taken directly from the SPARC catalogue. To assess possible projection or extinction-related systematics, the sample is additionally divided into three inclination ranges: low-inclination systems ($i < 45°$), intermediate-inclination systems ($45° \leq i < 70°$), and high-inclination systems ($i \geq 70°$). Inclination is treated strictly as a control variable and plays no role in the prediction of galaxy colors.

3 Model and Predicted Quantities

3.1 Stellar population reconstruction

For each galaxy, the model reconstructs a synthetic stellar population whose gravitational contribution reproduces the radial distribution of the missing mass component required to explain the observed rotation curve. No photometric information, spectral energy distribution, or observed color is used at any stage of the reconstruction.

More specifically, the reconstruction relies only on the radial profile of the baryonic mass and the missing mass inferred from the rotation curve, represented by the set of points $(M_{\rm bar}(r), M_{\rm dark}(r), r)$. This profile is treated as the sole galaxy-specific input to the model.

The synthetic population is described as a mixture of stellar components, including compact remnants (black holes, neutron stars, white dwarfs), red giants, and main-sequence stars spanning the usual spectral classes from O to M. Each component is characterized by a fixed representative mass density. The model explores variations in the relative mass fractions of these components as a function of galactocentric radius, under the constraint that their combined gravitational potential reproduces the required missing mass distribution.

These components are not selected to reproduce a realistic spectral or photometric population, nor an initial mass function. Instead, they are chosen to span a wide range of intrinsic mass densities, providing a flexible basis for reconstructing the gravitational mass profile through its dynamical influence.

The reconstruction is independent of the observed colors and relies exclusively on the dynamical constraints. For a given missing mass profile, the reconstruction procedure is fully deterministic and yields a unique stellar population composition, fixed by the dynamical inputs.

3.2 Predicted photometric quantities

Once the stellar population has been reconstructed from the dynamical constraints alone, its integrated photometric properties are computed. This step constitutes a forward modeling

stage, in which the reconstructed population is translated into observable quantities without any additional adjustment.

For each stellar component of the reconstructed population, standard stellar population synthesis prescriptions [9, 10] are used to assign spectral energy distributions consistent with the corresponding stellar class. The total emission of a galaxy is then obtained by summing the contributions of all components, weighted by their reconstructed mass fractions.

From the resulting integrated spectrum, global photometric quantities are derived, including ultraviolet and optical colors. In particular, the color indices FUV–NUV, $g-r$, $r-z$, and NUV–r are computed in a fully self-consistent manner. These predicted colors depend exclusively on the reconstructed stellar population and do not involve any photometric input from the observed data.

More specifically, the reconstruction relies only on the radial distribution of the baryonic mass and the missing mass component required to reproduce the observed dynamics, i.e. the set of points $(M_{\rm bar}(r), M_{\rm dark}(r), r)$ inferred from the rotation curve. The predicted photometric quantities therefore constitute genuine outputs of the model, which are subsequently compared to the observed GALEX and SDSS measurements in a purely a posteriori fashion.

3.3 Statistical comparison and robustness tests

The predicted photometric quantities are compared to the observed GALEX and SDSS measurements using a set of complementary statistical indicators designed to assess both the strength and the robustness of the inferred relations. All statistical analyses are performed on global galaxy-integrated quantities.

The primary level of comparison relies on correlation analyses between predicted and observed colors. Both Pearson linear correlation coefficients and Spearman [11, 12] rank-order correlation coefficients are computed. The Pearson coefficient probes linear associations in the raw photometric space, while the Spearman coefficient is sensitive to monotonic ordering independently of the absolute scaling. Statistical significances are expressed in terms of equivalent Gaussian standard deviations.

In order to control for potential observational biases, residuals between observed and predicted colors are examined as a function of galaxy inclination. Both signed and absolute residuals are tested for correlation with inclination angle, allowing the identification of possible systematics associated with projection effects or dust attenuation [13]. These tests are applied consistently across all color indices.

The robustness of the detected correlations is further quantified using resampling techniques. Bootstrap resampling is employed to estimate the distribution of correlation coefficients under repeated random sampling with replacement, providing confidence intervals and sign stability diagnostics. In parallel, jackknife resampling is used to estimate the sensitivity of the results to individual galaxies and to compute independent standard error estimates [14–16].

In addition, non-parametric permutation tests [17] are performed to assess the probability of obtaining correlation coefficients at least as extreme as the observed ones under the null hypothesis of no association. Observed values are compared to distributions obtained from random permutations of the photometric data, yielding two-sided p-values that do not rely on asymptotic assumptions.

To further investigate the physical origin of the correlations, the sample is partitioned according to galaxy inclination and morphological type. The full statistical analysis is repeated independently within each subsample. This procedure allows one to verify whether

Table 1. Correlation analysis between predicted and observed galaxy colors. Pearson r and Spearman ρ coefficients are reported together with their Gaussian-equivalent significances. Linear fits are reported in rank–rank space.

Color	N	$r_{\rm P}$	$\sigma_{\rm P}$	$\rho_{\rm S}$	$\sigma_{\rm S}$	$b_{\rm rank} \pm 1\sigma$
$r-z$	129	0.159	1.81	0.437	5.47	0.437 ± 0.080
$g-r$	128	0.487	6.25	0.605	8.54	0.605 ± 0.071
FUV–NUV	136	-0.192	2.27	-0.357	4.43	-0.357 ± 0.081
NUV–r	119	0.493	6.13	0.631	8.79	0.631 ± 0.072

the detected relations persist across different dynamical configurations and morphological classes, and to discriminate genuine structural trends from population-dependent effects.

Together, these complementary tests provide a comprehensive assessment of the statistical significance, robustness, and internal consistency of the relations between dynamically predicted stellar populations and observed photometric properties.

4 Results

We begin by presenting the global ordering relations between the predicted stellar population properties and the observed photometric colors. Figure 1 shows the rank–rank scatter plots for the four color indices considered in this work: the optical colors $g-r$ and $r-z$, the ultraviolet color FUV $-$ NUV, and the mixed UV–optical color NUV $- r$.

In all cases, the predicted quantities are derived exclusively from the reconstructed stellar populations inferred from galactic dynamics, while the observed ranks are computed from GALEX and SDSS photometry. The diagonal line indicates the identity relation between predicted and observed ranks.

Table 1 summarizes the statistical correlations between the predicted global colors obtained from the reconstructed stellar populations and the observed photometric colors from GALEX and SDSS. For each color index, both Pearson and Spearman correlation coefficients are reported together with their Gaussian-equivalent significances, providing complementary information on linear and monotonic relationships. Linear regressions are performed in rank–rank space, which is particularly relevant for assessing the robustness of the predicted galaxy ordering independently of absolute photometric calibration.

The four panels reveal systematic relationships between predicted and observed colors, whose structure and strength depend on wavelength. Optical and UV–optical colors display clear monotonic trends, reflected by strong and highly significant rank correlations. In contrast, the purely ultraviolet color does not follow a single monotonic sequence: its rank–rank diagram exhibits a cross–like pattern, indicating the superposition of two opposite trends rather than a simple global correlation. Despite this complexity, the UV relation remains statistically significant, revealing a structured but multi–regime behavior.

The strongest correlations are obtained for the optical $g-r$ and UV–optical NUV–r colors, with Spearman coefficients $\rho = 0.61$ and $\rho = 0.63$, corresponding to significances above 8σ. The $r-z$ color exhibits a weaker but still highly significant monotonic correlation, while the purely ultraviolet FUV–NUV index shows a moderate anticorrelation.

Linear fits performed in rank–rank space yield slopes consistent with the measured Spearman coefficients, as expected for monotonic relations. In contrast, when the same relations

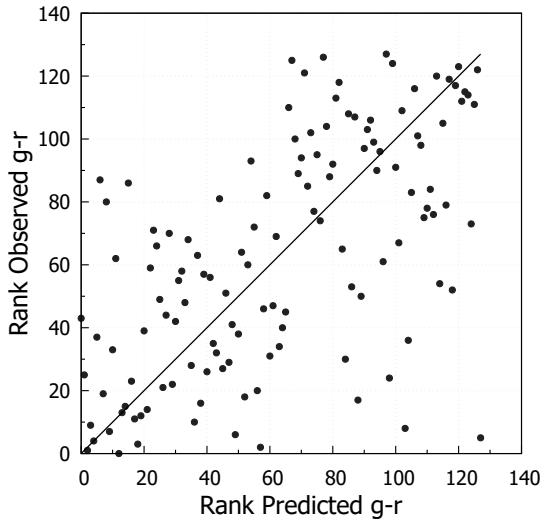

(a) $g - r$ color

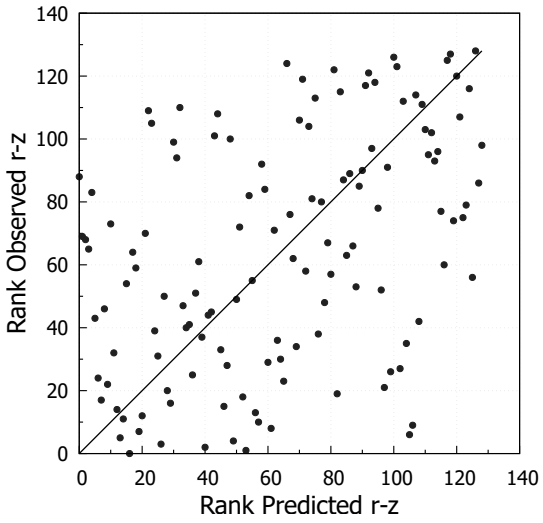

(b) $r - z$ color

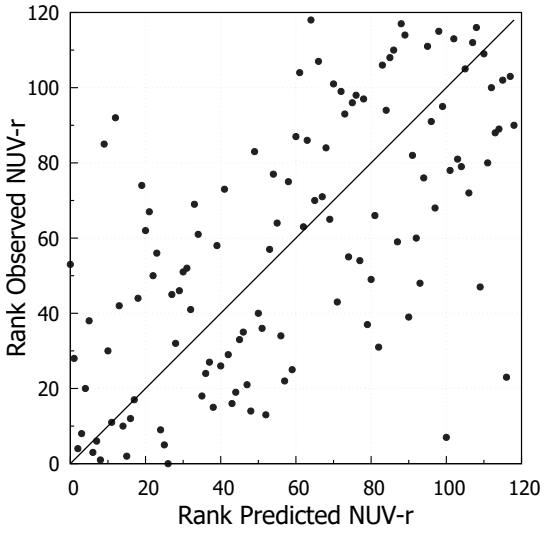

(c) NUV $- r$ color

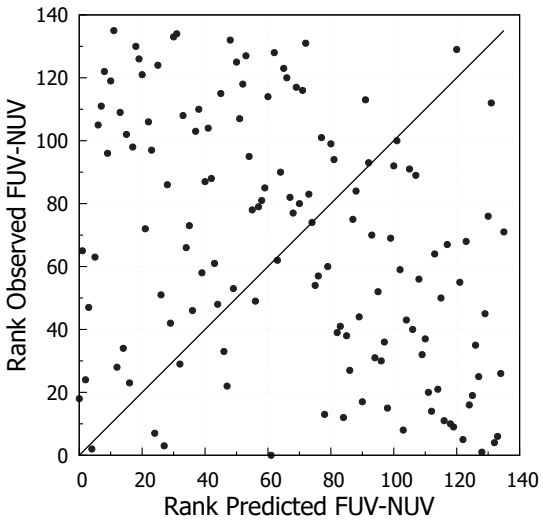

(d) FUV $-$ NUV color

Figure 1. Rank–rank comparison between predicted and observed photometric colors. Each point corresponds to one galaxy.

are examined in raw color space (see Appendix A), they exhibit substantial scatter and weak linear coherence. This indicates that the primary information carried by the model lies in the relative ordering of galaxies rather than in absolute color amplitudes.

4.1 Statistical robustness of the global correlations

Before investigating possible systematic effects related to inclination or morphology, we first assess the intrinsic robustness of the global correlations identified. This is achieved through

Table 2. Bootstrap and jackknife robustness analysis of the global color correlations. Bootstrap intervals correspond to the 16th, 50th, and 84th percentiles. The sign-flip fraction indicates the proportion of bootstrap realizations with opposite correlation sign.

Color	N	$r_{\rm P}$	$\rho_{\rm S}$	Bootstrap $\rho_{\rm S}$ (16/50/84)	Sign flip	Jackknife SE
$r-z$	129	0.159	0.443	[0.371, 0.443, 0.508]	0	0.068
$g-r$	128	0.487	0.598	[0.530, 0.597, 0.660]	0	0.066
FUV–NUV	136	−0.192	−0.366	[−0.451, −0.366, −0.277]	0	0.085
NUV–r	119	0.493	0.629	[0.564, 0.627, 0.684]	0	0.060

a combination of bootstrap resampling and jackknife estimation applied to the full galaxy sample for each color index.

For each color, bootstrap realizations are generated by resampling the galaxy set with replacement, and the distributions of Pearson and Spearman correlation coefficients are examined. The reported percentiles (16th, 50th, and 84th) provide an empirical estimate of the statistical dispersion around the nominal correlation. In parallel, jackknife resampling is used to estimate the sensitivity of the correlation coefficients to individual data points, yielding an independent estimate of the standard error.

Table 2 summarizes the results of this analysis. For all four colors, the bootstrap median values are fully consistent with the correlation coefficients measured on the full sample. The bootstrap distributions remain well separated from zero for the optical and UV–optical colors, and the fraction of bootstrap realizations exhibiting a sign reversal is negligible or null. This demonstrates that the detected correlations are not driven by a small subset of galaxies.

The purely ultraviolet color FUV–NUV displays broader bootstrap distributions and larger jackknife uncertainties, reflecting the more complex structure of its rank–rank relation. Nevertheless, the anticorrelation remains stable across resampling procedures, confirming that the signal is not a statistical artifact.

Overall, these resampling tests establish that the ordering relations identified in the full sample are statistically robust. This provides a solid foundation for the subsequent analysis of systematic effects related to inclination and morphological type.

4.2 Permutation tests

To complement the resampling analysis presented above, we perform permutation tests in order to assess the statistical significance of the observed correlations without relying on Gaussian assumptions. For each color index, the association between predicted and observed quantities is tested against the null hypothesis of no correlation by randomly permuting the observed values while keeping the predicted values fixed.

For each test, 10^5 random permutations are generated. The two–sided p–value is estimated as the fraction of permutations producing a correlation coefficient with absolute value greater than or equal to the observed one. For convenience of comparison with standard significance levels, the resulting p–values are also expressed as Gaussian–equivalent significances.

The results are summarized in Table 3. For all colors, the permutation tests confirm the trends identified in the rank–rank diagrams. The strongest correlations, corresponding to the optical $g-r$ and UV–optical NUV–r colors, are detected at very high significance for both Pearson and Spearman statistics, reaching the maximum significance accessible given the number of permutations. The $r-z$ color shows a weaker linear correlation, consistent

Table 3. Permutation test results for the global color correlations. Two–sided p–values are reported together with their Gaussian equivalent significances. For permutation tests with $p < 10^{-5}$, the reported significance corresponds to a lower bound set by the number of permutations.

Color	N	r_{P}	p_{P}	σ_{P}	ρ_{S}	σ_{S}
$r-z$	129	0.159	0.069	1.82	0.443	> 4.4
$g-r$	128	0.487	$< 10^{-5}$	4.41	0.598	> 4.4
FUV–NUV	136	-0.192	0.032	2.15	-0.366	4.17
NUV–r	119	0.493	$< 10^{-5}$	4.41	0.629	> 4.4

with the bootstrap analysis, but its rank correlation remains highly significant. The purely ultraviolet FUV–NUV color exhibits a statistically significant anticorrelation, despite its more complex, multi–regime structure.

Overall, the permutation tests demonstrate that the observed ordering relations are extremely unlikely to arise from random associations. This establishes the statistical reality of the correlations prior to any investigation of systematic effects related to inclination or morphology.

4.3 Inclination systematics

A potential concern in the interpretation of photometric correlations is the role of galaxy inclination, which can affect observed colors through dust attenuation, projection effects, and internal extinction. To assess whether the ordering relations identified above are driven by such systematics, we explicitly examine the dependence of the correlations on the inclination angle.

Figure 2 displays the rank–rank relations for the $g-r$ and NUV–r colors, with each galaxy encoded by its inclination angle in grayscale. No segregation of points along the inclination axis is observed that could account for the global monotonic trends. In particular, galaxies with similar predicted ranks span a wide range of inclinations, indicating that the primary ordering is not set by viewing geometry.

This conclusion is reinforced by direct correlation tests between inclination and the color residuals. For all four color indices, both Pearson and Spearman coefficients between the residuals and inclination remain significantly weaker than the main predicted–observed correlations. Although modest correlations are detected in some cases, especially in the ultraviolet bands, their amplitudes are insufficient to reproduce the observed rank–rank relations.

A purely kinematic origin of the optical correlations, such as a Doppler-related bias, is therefore strongly disfavored: the ordering persists in low-inclination systems, shows no monotonic dependence on inclination, and does not extend uniformly across wavelength bands.

Additional robustness is obtained by splitting the sample into low-, mid-, and high-inclination subsamples. Within each inclination bin, the monotonic ordering between predicted and observed colors persists, with comparable Spearman coefficients and consistent statistical significance. This demonstrates that the correlations are not driven by a specific inclination regime, nor by a small subset of highly inclined systems.

Taken together, these results show that inclination effects may modulate the scatter, particularly in the ultraviolet, but do not generate the observed ordering relations. The dominant signal therefore reflects an intrinsic connection between the dynamically inferred

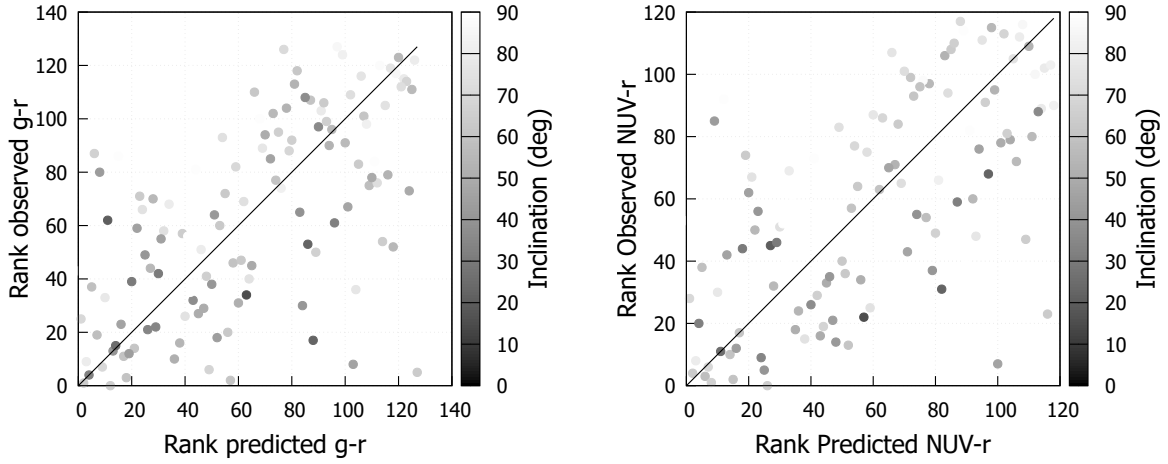

Figure 2. Rank–rank comparison between predicted and observed colors. Left: optical $g-r$. Right: UV–optical $NUV-r$. In both panels, the gray level encodes galaxy inclination.

stellar populations and the global photometric properties of galaxies, rather than a projection-induced bias.

4.4 Inclination-controlled subsamples

To further assess the impact of viewing geometry, the galaxy sample is divided into three inclination bins: low-inclination systems ($i < 45°$), intermediate inclinations ($45° \leq i < 70°$), and highly inclined galaxies ($i \geq 70°$). Correlation analyses are repeated independently within each subsample for all four color indices using the same statistical procedures as in the full sample, including permutation tests and bootstrap resampling.

Across optical and UV–optical colors, the predicted–observed ordering remains detectable within each inclination bin. While the statistical significance decreases for the low-inclination subsamples, primarily due to reduced sample sizes, the measured Spearman coefficients are fully consistent with those obtained for the full sample. In particular, the $g-r$ and NUV–r colors exhibit strong and highly significant monotonic correlations at intermediate and high inclinations, with $\rho \gtrsim 0.55$ and permutation-based significances exceeding 4σ.

The purely ultraviolet FUV–NUV color displays a more complex behavior. At low inclinations, no statistically significant correlation is detected, whereas intermediate and high-inclination subsamples reveal increasingly strong anticorrelations. This trend mirrors the cross-like structure observed in the global rank–rank diagram and suggests the coexistence of multiple ultraviolet regimes rather than a single monotonic relation.

Overall, these results demonstrate that inclination does not drive the observed ordering relations. Instead, inclination acts primarily as a secondary source of scatter, especially in the ultraviolet, while the dominant correlations originate from intrinsic galaxy properties encoded in the dynamical reconstruction.

Table 4. Inclination-controlled Spearman rank correlations between predicted and observed colors. Results are reported for low ($i < 45°$), intermediate ($45° \leq i < 70°$), and high ($i \geq 70°$) inclination subsamples. Uncertainties correspond to bootstrap 68% intervals.

Color	Inclination bin	N	ρ_S	Significance
$r - z$	Low	23	0.57 ± 0.15	2.8σ
	Mid	62	0.36 ± 0.11	2.9σ
	High	44	0.52 ± 0.10	3.6σ
$g - r$	Low	23	0.39 ± 0.24	1.8σ
	Mid	61	0.58 ± 0.10	4.4σ
	High	44	0.69 ± 0.10	$> 4\sigma$
FUV–NUV	Low	26	0.08 ± 0.20	n.s.
	Mid	64	-0.50 ± 0.12	4.3σ
	High	46	-0.54 ± 0.11	4.0σ
NUV–r	Low	21	0.38 ± 0.25	n.s.
	Mid	55	0.65 ± 0.10	$> 4\sigma$
	High	43	0.66 ± 0.09	4.3σ

4.5 Morphology-controlled subsamples

Unlike inclination, morphological type is a discrete and partially subjective classification, for which no meaningful continuous residual correlation can be defined. Morphological systematics are therefore investigated exclusively through controlled subsample analyses.

To further assess the robustness of the ordering relations, the galaxy sample is divided according to Hubble morphological type. Three broad classes are considered: early-type disks (S0–Sb), late-type spirals (Sbc–Sdm), and irregular systems (Sm–BCD). For each class, the correlation analysis is repeated independently using the same statistical procedures as in the full sample, including permutation tests and bootstrap resampling.

For optical colors, the strength of the correlation depends markedly on morphology. In the $r - z$ color, no significant ordering is detected for early-type disks or irregular galaxies, while late-type spirals exhibit a clear monotonic relation with a Spearman coefficient $\rho = 0.29$, corresponding to a permutation-based significance of 2.2σ. A similar behavior is observed for the $g - r$ color, where the ordering is strongly significant in late-type spirals ($\rho = 0.51$, $> 4\sigma$), marginal in early-type disks, and absent in irregular systems.

The ultraviolet color FUV–NUV does not show statistically significant correlations in any morphological class. Bootstrap and permutation tests indicate that the apparent trends observed in the global sample result from the superposition of opposite behaviors across morphological types, rather than from a single monotonic relation within each class.

In contrast, the UV–optical color NUV–r exhibits a robust and highly significant ordering within late-type spirals, with Spearman $\rho = 0.51$ and a significance close to 4σ. Early-type disks show no detectable monotonic relation, while irregular galaxies display a weaker but still statistically significant correlation at the $\sim 2.4\sigma$ level.

Overall, these results demonstrate that the strongest ordering relations are intrinsic to disk-dominated systems, particularly late-type spirals. The absence of significant correlations in irregular galaxies and early-type disks rules out a trivial morphological segregation as

Table 5. Morphology-controlled correlation analysis between predicted and observed colors. Spearman coefficients and Gaussian-equivalent significances are derived from permutation tests.

Color	Morphology	N	ρ_S	Significance
$r-z$	S0–Sb	20	0.14	0.6σ
	Sbc–Sdm	59	0.29	2.2σ
	Sm–BCD	50	0.08	0.5σ
$g-r$	S0–Sb	20	0.19	0.8σ
	Sbc–Sdm	58	0.51	4.1σ
	Sm–BCD	50	0.22	1.5σ
FUV–NUV	S0–Sb	25	−0.08	0.4σ
	Sbc–Sdm	58	−0.20	1.5σ
	Sm–BCD	53	−0.23	1.6σ
NUV–r	S0–Sb	18	0.03	0.1σ
	Sbc–Sdm	55	0.51	3.8σ
	Sm–BCD	46	0.35	2.4σ

the origin of the global signal. Instead, the observed ordering reflects a genuine connection between galactic dynamics and stellar population properties within structurally comparable systems.

5 Discussion

5.1 Origin of the ordering

The ordering relations identified in this work do not arise from any explicit use of photometric information, nor from a direct constraint on global stellar properties. Instead, they emerge from the internal structure of the reconstruction algorithm, which builds the stellar population distribution through a sequential and locally constrained procedure along the radial dimension [18].

The reconstruction starts from the innermost galactocentric radius for which the dynamical constraint is best resolved. At this initial radius, a local stellar population mixture is determined so as to reproduce the required amount of the baryonic mass and the missing mass inferred from the rotation curve. This solution constitutes the first fully specified population state of the galaxy.

Crucially, this local solution is not discarded when moving to neighboring radii. Instead, it is propagated outward and used as the initial population distribution for the resolution at the next radial point. At each subsequent radius, the algorithm performs a local adjustment of the stellar population mixture, starting from the previously obtained solution and modifying it only as required to satisfy the new dynamical constraint.

This procedure enforces a strong continuity of the solution along the radial direction. The stellar population at a given radius is therefore not an independent fit, but a locally corrected continuation of the population determined at smaller radii. As a consequence, abrupt or arbitrary changes in the population mixture are suppressed, and the solution evolves smoothly as a function of radius.

The impact of this continuity is amplified by the strongly non–linear response of the reconstructed mass contribution to the intrinsic densities of the stellar components. Because different stellar populations contribute very differently to the missing mass budget, even small local adjustments can have significant effects, while remaining constrained by the inherited population state. This non–linearity limits the range of admissible corrections at each step and progressively restricts the accessible solution space.

By the time the reconstruction reaches the outermost radii, corresponding effectively to the total missing mass of the galaxy, the stellar population distribution has already undergone a sequence of locally constrained adjustments. The final global population is therefore not the result of a single global fit, but the cumulative outcome of a chain of dependent local solutions.

When integrated into predicted photometric quantities, these coherently constructed stellar populations naturally produce systematic variations in global colors. The observed ordering between galaxies thus reflects the structured propagation of dynamical constraints through the reconstruction algorithm, rather than an imposed monotonic relation or a tuning to match observed photometric trends.

Because the analysis relies on rank-based statistics and does not involve luminosity as an input or output, the observed relations cannot be interpreted as a Tully–Fisher–like scaling

5.2 Limitations and scope

Despite the strength and robustness of the detected ordering relations, several limitations of the present approach must be emphasized.

First, the reconstruction of stellar populations is not intended to represent a full physical model of star formation or chemical evolution. Processes such as gas accretion, feedback, and environmental interactions are not explicitly modeled. Instead, the approach provides an effective description of the integrated stellar content constrained by the dynamical mass distribution. As a consequence, the model is not expected to reproduce absolute photometric values with high precision, but rather the relative organization of galaxies in color space.

Second, the method relies on the availability and quality of resolved rotation curves. Galaxies with poorly constrained dynamics or strong non-circular motions fall outside the scope of the present analysis. The results therefore apply primarily to disk galaxies with well–measured rotation curves, as provided by the SPARC sample.

Third, while extensive robustness tests demonstrate that the detected correlations are not driven by inclination or morphology alone, these factors still introduce secondary modulations. The inclination–controlled and morphology–controlled subsamples reveal that the strength of the ordering varies across galaxy classes, particularly in the ultraviolet bands. This indicates that additional physical parameters, not explicitly included in the reconstruction, contribute to shaping the detailed photometric properties.

Finally, the present study is restricted to local galaxies. The extent to which similar ordering relations persist at higher redshift, where galaxies experience more rapid evolutionary processes, remains an open question. Future applications to resolved photometry, spectral energy distributions, and evolving galaxy samples will be required to assess the generality of the proposed framework.

Within these limitations, the results demonstrate that galactic dynamics alone contain sufficient information to recover a significant and physically meaningful ordering of stellar populations. This finding suggests a deeper structural link between gravitational dynamics and the integrated properties of galaxies, which merits further investigation.

6 Conclusion

In this work, we have shown that a significant ordering of global stellar population properties can be recovered directly from galactic dynamics, without any use of photometric information in the reconstruction procedure. Predicted integrated colors, derived solely from stellar populations inferred from rotation curves, exhibit statistically robust correlations with observed GALEX and SDSS photometry across optical, ultraviolet, and mixed UV–optical bands.

The analysis demonstrates that this agreement is not limited to a single correlation metric or wavelength range. Strong monotonic relations are observed for the optical $g - r$ and UV–optical NUV–r colors, while the purely ultraviolet FUV–NUV index displays a more complex, multi–regime structure. Bootstrap resampling and permutation tests confirm that these relations are stable and highly unlikely to arise from random fluctuations.

Systematic effects related to galaxy inclination and morphology have been explicitly examined. While inclination introduces measurable secondary trends in the residuals, the primary ordering between predicted and observed colors persists within inclination–controlled and morphology–controlled subsamples. This indicates that the detected relations are not driven by observational projection effects or by a single morphological class, but reflect a more general structural connection.

The origin of the ordering lies in the reconstruction algorithm itself. The stellar population is determined through a sequential, radially propagated procedure in which each local solution serves as the initial condition for the next. Combined with the non–linear dependence of the reconstructed mass contribution on stellar component densities, this induces a coherent and constrained evolution of the population distribution across the galaxy. The final global stellar population is therefore the cumulative result of a series of locally constrained adjustments rather than a single global fit.

Taken together, these results demonstrate that the relative ordering of galaxies in integrated color space can be recovered from dynamical information alone. This establishes a direct empirical link between galactic dynamics and stellar population properties, independent of photometric calibration or population synthesis tuning. The approach opens new perspectives for probing stellar populations in systems where photometric data are incomplete or uncertain, and suggests that a significant fraction of the information traditionally inferred from colors is already encoded in the dynamical structure of galaxies.

Software availability

The C++ program used to perform all numerical calculations and generate the corresponding graphs are freely available at dark-mass-generator.sourceforge.io or at figshare.com/authors/Nicolas_Poupart/22566419.

Funding

This research received no specific grant from any funding agency in the public, commercial, or not-for-profit sectors.

Competing interests

The author declares no competing interests.

Roles

The author conceived the study, performed the analysis, and wrote the manuscript.

A Raw predicted versus observed color relations

For completeness, we present in this appendix the direct scatter plots between predicted and observed global colors, shown in linear (non–ranked) space. These figures complement the rank–rank analysis discussed in the main text by illustrating the dispersion and non–linear structure of the relations in absolute color units.

While the absolute correlations are weaker than their rank–based counterparts, these diagrams provide a visual reference for the intrinsic scatter, saturation effects, and non–Gaussian features present in the data.

References

[1] V.C. Rubin, J. Ford, W. Kent and N. Thonnard, *Rotational properties of 21 sc galaxies with a large range of luminosities and radii, from ngc 4605 (r = 4kpc) to ugc 2885 (r = 122kpc)*, *The Astrophysical Journal* **238** (1980) 471.

[2] A. Bosma, *The distribution and kinematics of neutral hydrogen in spiral galaxies of various morphological types*, *PhD thesis, Rijksuniversiteit Groningen* (1978) .

[3] C. Conroy, *Modeling the panchromatic spectral energy distributions of galaxies*, *Annual Review of Astronomy and Astrophysics* **51** (2013) 393.

[4] F. Lelli, S.S. McGaugh and J.M. Schombert, *Sparc: Mass models for 175 disk galaxies with spitzer photometry and accurate rotation curves*, *The Astronomical Journal* **152** (2016) 157.

[5] D.C. Martin et al., *The galaxy evolution explorer: A space ultraviolet survey mission*, *The Astrophysical Journal Letters* **619** (2005) L1.

[6] L. Bianchi et al., "Galex gr5 x sdss dr7 matched catalogs." MAST / STScI High-Level Science Products, 2011.

[7] D.G. York et al., *The sloan digital sky survey: Technical summary*, *The Astronomical Journal* **120** (2000) 1579.

[8] M. Fukugita, T. Ichikawa, J.E. Gunn, M. Doi, K. Shimasaku and D.P. Schneider, *The sloan digital sky survey photometric system*, *The Astronomical Journal* **111** (1996) 1748.

[9] G. Bruzual and S. Charlot, *Stellar population synthesis at the resolution of 2003*, *Monthly Notices of the Royal Astronomical Society* **344** (2003) 1000.

[10] C. Conroy, J.E. Gunn and M. White, *The propagation of uncertainties in stellar population synthesis modeling. i. the stellar initial mass function, stellar evolution, and stellar spectral libraries*, *The Astrophysical Journal* **699** (2009) 486.

[11] K. Pearson, *Note on regression and inheritance in the case of two parents*, *Proceedings of the Royal Society of London* **58** (1895) 240.

[12] C. Spearman, *The proof and measurement of association between two things*, *The American Journal of Psychology* **15** (1904) 72.

[13] R.B. Tully, M.J. Pierce, J.-S. Huang, W. Saunders, M.A.W. Verheijen and P.L. Witchalls, *Global extinction in spiral galaxies*, *The Astronomical Journal* **115** (1998) 2264.

[14] B. Efron and R.J. Tibshirani, *An Introduction to the Bootstrap*, Chapman and Hall/CRC (1993).

[15] M.H. Quenouille, *Approximate tests of correlation in time-series*, *Journal of the Royal Statistical Society. Series B* **11** (1949) 68.

[16] J.W. Tukey, *Bias and confidence in not-quite large samples*, *Annals of Mathematical Statistics* (1958) .

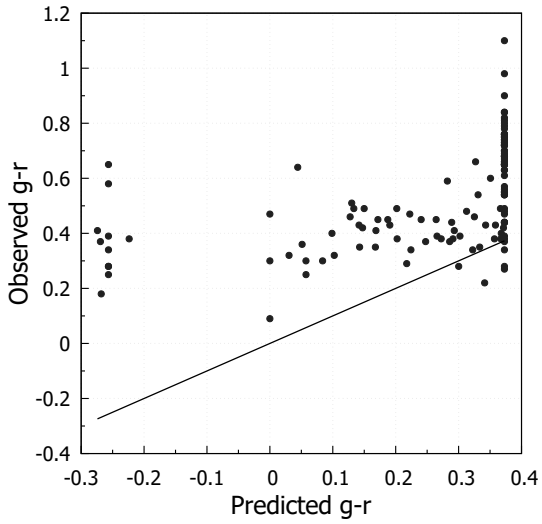

(a) Predicted versus observed $g - r$ color

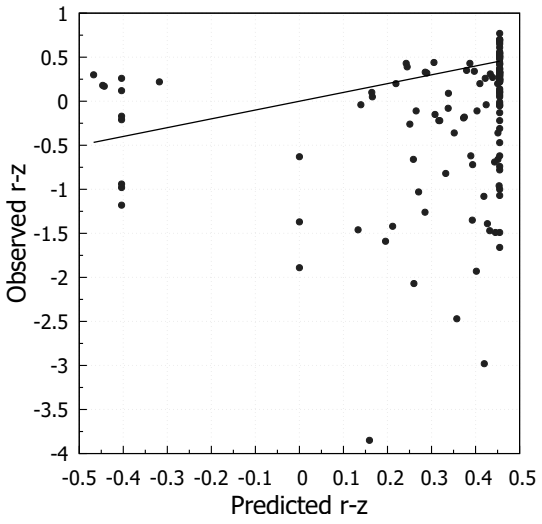

(b) Predicted versus observed $r - z$ color

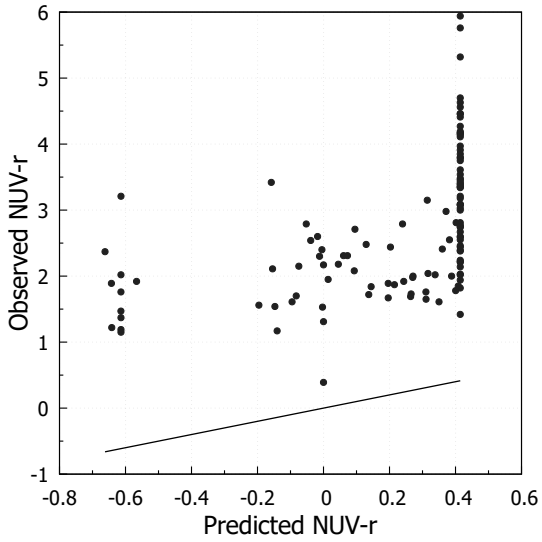

(c) Predicted versus observed NUV $- r$ color

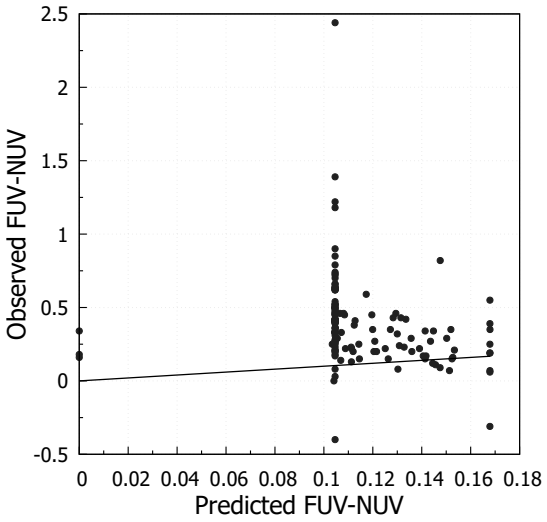

(d) Predicted versus observed FUV $-$ NUV color

Figure 3. Direct comparison between predicted and observed global colors in linear space. Each point corresponds to one galaxy. The diagonal line corresponds to the identity relation $y = x$ and is shown only as a visual reference for absolute agreement. These plots highlight the substantial intrinsic scatter in absolute color space, motivating the use of rank–based statistics in the main analysis.

[17] P.I. Good, *Permutation, Parametric, and Bootstrap Tests of Hypotheses*, Springer, 3 ed. (2005).

[18] N. Poupart, "Dark mass is potential energy." Preprint available at FigShare (doi.org/10.6084/m9.figshare.30543407) and ResearchGate (doi.org/10.13140/RG.2.2.15355.43046), 2025.